Remote Sensing Of Environment
July 2015, Volume 164 Pages 225-237
http://dx.doi.org/10.1016/j.rse.2015.03.030
http://archimer.ifremer.fr/doc/00269/37998/

Detection of mesoscale thermal fronts from 4km data using smoothing techniques: Gradient-based fronts classification and basin scale application

Roa Pascuali Liliana [1, *], Demarcq Herve [1], Nieblas Anne-Elise [2]

[1] Univ Montpellier, CNRS, Inst Francais Rech Exploitat Mer IFREMER, Inst Rech Dev,UMR MARBEC,Ifremer,Stn Ifremer, F-34203 Sete, France.
[2] Univ Montpellier, CNRS, Inst Francais Rech Exploitat Mer IFREMER, UMR MARBEC,IRD,Ifremer,Stn Ifremer, F-34203 Sete, France.

* Corresponding author : Liliana Roa Pascuali, Tel.: + 33 4 99 57 32 13. ; email addresses : liliana.pascuali@ird.fr ; lrpascuali@yahoo.com

Abstract :

In order to optimize frontal detection in sea surface temperature fields at 4 km resolution, a combined statistical and expert-based approach is applied to test different spatial smoothing of the data prior to the detection process. Fronts are usually detected at 1 km resolution using the histogram-based, single image edge detection (SIED) algorithm developed by Cayula and Cornillon in 1992, with a standard preliminary smoothing using a median filter and a 3 × 3 pixel kernel. Here, detections are performed in three study regions (off Morocco, the Mozambique Channel, and north-western Australia) and across the Indian Ocean basin using the combination of multiple windows (CMW) method developed by Nieto, Demarcq and McClatchie in 2012 which improves on the original Cayula and Cornillon algorithm. Detections at 4 km and 1 km of resolution are compared.

Fronts are divided in two intensity classes (“weak” and “strong”) according to their thermal gradient. A preliminary smoothing is applied prior to the detection using different convolutions: three type of filters (median, average and Gaussian) combined with four kernel sizes (3 × 3, 5 × 5, 7 × 7, and 9 × 9 pixels) and three detection window sizes (16 × 16, 24 × 24 and 32 × 32 pixels) to test the effect of these smoothing combinations on reducing the background noise of the data and therefore on improving the frontal detection. The performance of the combinations on 4 km data are evaluated using two criteria: detection efficiency and front length. We find that the optimal combination of preliminary smoothing parameters in enhancing detection efficiency and preserving front length includes a median filter, a 16 × 16 pixel window size, and a 5 × 5 pixel kernel for strong fronts and a 7 × 7 pixel kernel for weak fronts. Results show an improvement in detection performance (from largest to smallest window size) of 71% for strong fronts and 120% for weak fronts. Despite the small window used (16 × 16 pixels), the length of the fronts has been preserved relative to that found with 1 km data.

This optimal preliminary smoothing and the CMW detection algorithm on 4 km sea surface temperature data are then used to describe the spatial distribution of the monthly frequencies of occurrence for both strong and weak fronts across the Indian Ocean basin. In general strong fronts are observed in coastal areas whereas weak fronts, with some seasonal exceptions, are mainly located in the open ocean.

This study shows that adequate noise reduction done by a preliminary smoothing of the data considerably improves the frontal detection efficiency as well as the global quality of the results. Consequently, the use of 4 km data enables frontal detections similar to 1 km data (using a standard median 3 × 3 convolution) in terms of detectability, length and location. This method, using 4 km data is easily applicable to large regions or at the global scale with far less constraints of data manipulation and processing time relative to 1 km data.

Highlights

► We improve 4 km SST frontal detections with a preliminary gradient-based smoothing. ► Gradient-based smoothing is tested with multiple detection window sizes. ► Strong and weak fronts are defined based on their thermal gradient intensity. ► Improved detection performance at 4 km is comparable to 1 km data. ► The method is adequate to process large marine areas.

Keywords : Mesoscale thermal fronts, Preliminary smoothing, Sea surface temperature, 4 km resolution, Gradient intensity classification, Expert-based approach, Detection efficiency, Indian Ocean

1. Introduction

Fronts are constitutive elements of almost all spatial structures observed at the ocean surface worldwide. These boundaries are equally as important in characterizing the epipelagic environment as continuous surface descriptors, such as temperature, salinity and ocean color. Fronts are primarily driven by physical displacements of surface waters; thus, sea surface temperature (SST) is by far the parameter by which fronts are most often detected. Synoptic satellite observations enable fronts to be identified at regional or even basin scale, according to data processing capabilities.

There are two primary methods by which fronts are detected: the gradient-based approach and the histogram-based approach. The Canny operator (Canny, 1986) is the most commonly used gradient-based method. In general, this method applies an upper gradient threshold to identify a pixel as an edge and a lower threshold to discard it. If the pixel gradients are between both thresholds, only the pixels that is closest to the upper threshold are marked as an edge (i.e., skeletonization). The histogram-based approach detects the limit that divides two distinct pixel populations. The most commonly used method for this approach is the single edge detection algorithm (SIED) developed by (Cayula & Cornillon, 1992) that is based on a bimodal histogram of two water masses.

The SIED is developed in two main axes: the identification and correction of clouds and the edge detection itself. Prior to the detections, this method requires a standard preliminary smoothing of the images (generally using 1 km SST data), consisting of a 3×3 median filter in order to reduce the local noise. The detection process includes a division of the image into fixed windows of size 32×32 pixels, in which the algorithm searches for fronts. The algorithm examines the spatial properties of the SST field in each window to investigate the presence of a thermal limit between two water masses. Specifically, a SST histogram is computed from each window and tested for significant bimodality to determine if a frontal edge is present. Three internal parameters are defined by the SIED to formally identify a front: 1) the spatial cohesion threshold, $\theta = 0.90$, to test the bimodality, 2) the signal-to-noise ratio, $S = 4$, related to a maximum error probability and 3) the population threshold, $P_{wi} \geq 0.25$, that represents the minimum size ratio between water populations. The last stage of the analysis, termed the "following algorithm", joins contours that are slightly separated (Cayula & Cornillon, 1992).

Since 1992, many studies have developed upon the original Cayula and Cornillon method. In 1995, Cayula and Cornillon themselves applied their previous SIED algorithm to a sequence of SST images to develop the multi-image edge detector (MIED) method that simultaneously detects weaker fronts and improves the elimination of false detections.

Ullman and Cornillon (2000) evaluated different gradient and histogram-based edge detection algorithms using Advanced Very High Resolution Radiometer SST data and compared their results with SST fronts obtained from *in situ* data. They tested false front detections and failures to detect fronts and concluded that the false front error rates were less important for the SIED than for gradient-based method. They suggested that SIED frontal detection algorithm can be useful in providing accurate statistics of front occurrence at scales > 10 km, but that gradient-based methods were more accurate at scales < 10 km. Ullman and Cornillon (2001) then applied the MIED algorithm to 12 years of SST images, revealing the presence of persistent fronts off the northeast US coast.

Diehl et al. (2002) investigated an approach using "geographic window sizes" (window size is determined by the correlation of the data surrounding the window's central point) to avoid the limitation of the unique window size used by the SIED algorithm. They found that front detection is improved where fronts are smaller or more dense, mostly in coastal regions, but at a cost of a complex data re-composition.

In terms of expanding the SIED to other data types, Miller (2004, 2009a) was among the first to apply the

SIED to Sea-viewing Wide Field-of-view Sensor data to detect chlorophyll-*a* (Chla) fronts and boundaries of suspended matter. He combined these with SST fronts to describe the physical and biological interactions involved in coastal areas under tidal influence.

Using Chla data, Wall et al. (2008) applied a gradient-based and a histogram-based algorithm on the coastal waters off Florida, combining 32×32 and 16×16 pixel detection windows and modifying some SIED parameters. They found that the gradient-based algorithm was better at identifying near-shore Chla fronts than weaker offshore fronts.

More recently, Nieto et al. (2012) proposed an improved implementation of the Cayula and Cornillon (1992) algorithm termed the combination of multiple windows (CMW), initially applied to 1 km SST data. This method, used in the present study, applies grids of frontal detection (four 32×32 pixel windows) that overlap by half their size in order to overcome the edge effect of the original SIED algorithm, whose detection efficiency decreases towards the edges of the windows. This method provides huge improvements from the standard Cayula and Cornillon SIED approach in terms of both edge detection (140%) and front length (30%).

Prior to the detection of fronts, a pre-processing of the data based on smoothing filters is needed in order to remove the noise introduced by the sensor and the uncorrected atmospheric effects. The smoothing procedure helps to preserve valid information from the original noise (the high frequency signal in the spatial domain) by improving the quality of the subsequent frontal detection. At the same time, the selection of an adequate window size is critical for the performance of the detection. All methods based on SIED have been almost exclusively applied to 1 km data (and mostly SST data) that facilitates the tuning of the algorithm and supplies the most detailed and accurate results. They generally use similar preliminary smoothing methods (a median filter with a 3×3 kernel) and the 32×32 pixel window. Table 1 summarizes the data resolution, preliminary smoothing and internal parameters used by several authors in the application of the SIED method. The only study known to us that uses a different smoothing method is that by Belkin and O'Reilly (2009). This study applied a median filter that considers a small window (3×3 pixels) within a larger one (5×5 pixels) before the detection process applied to both SST and Chla data.

Table 1. Parameters applied in previous studies using the Cayula and Cornillon (1992) SIED algorithm to detect sea surface temperature and chlorophyll-*a* fronts from satellite images.

Authors	Year	Detection Method Applied	Res. (km)	Filter	Kernel	Window	θ	S/N	$P(w_i)$
Cayula and Cornillon	1992	SIED (Single image Edge Det.)	1	Median	3	32x32	0.9	4	0.25
Cayula and Cornillon	1995	MIED (Multiple IED)	1 and 2	Median	3	32x32	0.9	4	0.25
Ullman and Cornillon	1999	SIED	1	Median	3	32x32	-	-	-
Ullman and Cornillon	2000	SIED	1	Median	3	32x32	-	-	-
Dielh et al	2002	SIED + Geographic Win. approach	1	Median	3	variable	-	-	-
Belkin and Cornillon	2003	SIED	9	Median	3	32x32	-	-	-
Wall et al	2008	SIED CANNY Gradient-based algorithm	1	Median Gaussian	3	16x16, 32x32 3x3	0.95	4	0.25
Belkin and O'Reilly	2009	SIED, MIED	9	Median	3	32x32	-	-	-
Belkin	2009	Sobel gradient	1	Median	3	5x5	-	-	-
Miller	2004	SIED	9	Median	3	32x32	-	-	-
Miller	2009	SIED Composite front map approach		Median	3	32x32	-	-	-
Nieto et al	2012	SIED/Combination Multiple Windows	1	Median	5	32x32	0.7	3	0.15
This study	-	SIED/Combination Multiple Windows	4.4	Median	5 - 7	16x16	0.65	3	0.10

The objective of our study is to define an adequate pre-processing procedure to detect fronts using 4 km data without losing relevant information (e.g., general patterns, detection of weak fronts, coherence of detections, and length). The considerable advantage of such upscaling is the ability to process data at the basin or global scale, minimizing processing time and avoiding data handling constraints.

Thus, we extensively test frontal detections made with different combinations of preliminary smoothing parameters, including median, average, and Gaussian filters at four different kernel sizes (i.e., 3×3, 5×5, 7×7, and 9×9 pixels) and using different detection window sizes (16×16, 24×24, and 32×32 pixels). We aim to propose a new conditional smoothing method that maximizes edge detection quality from 4 km data.

We then perform a classification of the fronts at the basin scale, based on the intensity of their thermal gradient. The resulting patterns are described in particular for coastal and offshore regions, highlighting some oceanographic processes.

It is important to note that while we do not validate our frontal detections with *in-situ* measurements, we test the performance of the contextual smoothing method using 4 km data and consider all fronts that are detected to be real.

2. Methods.

2.1. Satellite data.

Daily 1 km and 4 km SST fields are obtained from the Moderate Resolution Imaging Spectroradiometer (MODIS) of the Aqua platform, for the period between 2002 and 2011 (http://oceancolor.gsfc.nasa.gov/). Another data set of 2 km resolution is sampled from 1 km data in order to analyze the variability of the frontal gradients according to different spatial resolutions (i.e., 1, 2 and 4 km). The quality flags available for 4 km (i.e., 0, 1 ,2) are tested to evaluate their effect on the detection of frontal structures. Flag 0 gathers initial detectability tests that are considered as a minimal requirement for pixels without cloud cover. Since flags 1 and 2 include a threshold that masks the highest SST gradients along with cloud borders, only flag 0 is kept.

2.2 Study areas.

Several regions around the world are used to test the effect of applying different smoothing parameters prior to the detections of fronts using the CMW method (Nieto et al., 2012) on 4 km data. Though the base algorithm for CMW, the SIED method, is known to have low sensitivity to cloud cover (Cayula & Cornillon, 1992), we select three areas of low cloud coverage to give a maximal spatial continuity in frontal detections. This allows us to measure the length of fronts that are detected, without spatial constraints. To test the effects of the preliminary smoothing methods, five clear images of each of the three areas (for a total of 15 days) are selected across ten years of data (about 10^7 pixels in total) in order to achieve statistically significant results. The resulting smoothing parameters are then applied and fronts are detected using the CMW method at the basin scale.

The study areas are each characterized by high mesoscale variability and include the region offshore of Morocco, the Mozambique Channel, and offshore of north-western Australia (Fig. 1). The Moroccan region, located between a rich coastal upwelling and offshore stratified oligotrophic waters, is influenced by the Canary Current (Fig. 1). The variable intensity of the upwelling is related to numerous coastal topographic irregularities which make mesoscale structures (and hence, fronts) very common in this region (Nieto et al., 2012; Pacheco & Hernandez-Guerra, 1999). The Mozambique Channel is influenced by the North Equatorial Madagascar Current that contributes to the southward Mozambique Channel flow and to the high eddy activity found in this region. The southern part of the channel is affected by the local upwelling of southern Madagascar and in Delagoa Bight (26-28°S) (Lutjeharms, 2006). The north-western Australian region is impacted by several currents, including the Indonesian Throughflow (ITF), the Halloway Current (HC) and the Leeuwin Current (LC) that act together to generates permanent high intensity coastal fronts (Fig. 1)

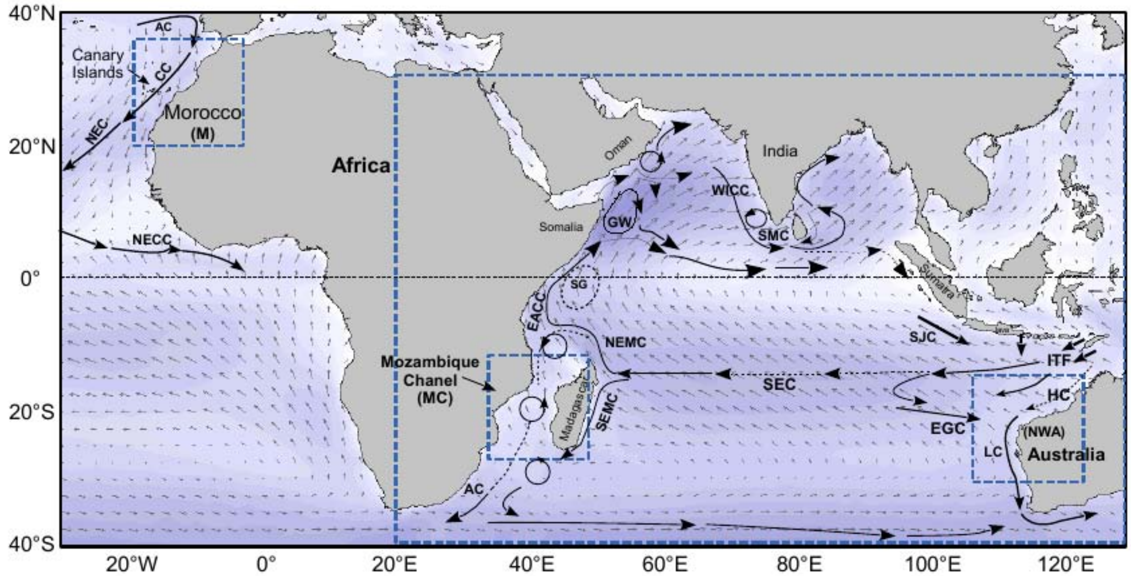

Figure 1. Mean wind velocity (June) and surface currents related to the three study areas: Morocco, Mozambique Channel and north-western Australia. Atlantic Ocean currents: Azores Current (AC), Canary Current (CC), North Equatorial Current (NEC), North Equatorial Counter Current (NECC). Indian Ocean currents: Great Whirl (GW), West Indian Coastal Current (WICC), South Monsoon Current (SMC), Southern Gyre (SG). Northeast and Southeast Madagascar Current (NEMC, SEMC), East African Coastal Current (EACC), Agulhas Current (AC), South Equatorial Current (SEC), East Gyral Current (EGC), South Java Current (SJC), Halloway Current (HC), Indonesian Throughflow (ITF) and Leeuwin Current (LC).

2.3 Frontal detection and assessment of preliminary data smoothing

The default data smoothing generally applied to the data prior to the frontal detection consists of a simple 3×3 median filter (as in Cayula & Cornillon (1992), see Table 1). Nevertheless, preliminary tests (not shown) indicate that the performance of the frontal detection greatly depends on the type and intensity of the smoothing applied, independent of the internal settings of the SIED algorithm.

In this study, we evaluate the practical effects of smoothing on frontal detection performance, including the influence of the local gradient whose intensity is directly related to the ability to detect fronts. We propose here to use the local gradient as an intrinsic property of the fronts in order to separate them into "weak" and "strong" categories. To do this we first apply a 3×3 Gaussian filter to reduce local noise and then determine the minimum significant surface gradient in our data, as measured by the Sobel operator (Gonzalez & Woods, 2007). Considering the effective radiometric resolution of the SST data (0.15°C) and the maximum size of a pixel in an equidistant cylindrical projection at the equator (4.5 km), the weakest (bi-directional) Sobel gradient (as measured linearly in a 3×3 pixel matrix) is close to 0.017°C km^{-1}.

Since residual uncorrected atmospheric artifacts tend to increase the measured gradient, we consider that 0.02°C km^{-1} is an adequate threshold to define significant SST gradients. We also confirm by visual expertise that gradients <0.02°C km^{-1} are generally associated with the background noise of the data and do not reveal interpretable oceanic structures.

Ultimately, we divide the fronts into two populations, separated by the mode of their distribution, thereafter labeled "weak" and "strong" fronts. The gradient associated with each frontal pixel is defined as the highest gradient value found at a maximum distance of three pixels from the front. This is done to account for the frequent slight spatial mismatch observed between the front position and its associated gradient. In order to define a representative threshold value for each type of fronts, the mode of the distribution is computed from a very large data set (in our case, one full year of daily data for the whole Indian Ocean, i.e., about 10^9 pixels). The median gradient value found is 0.042 °C km^{-1}. This value is then used as a reference for all regions of this study.

We then test the effects of different smoothing methods, or convolutions, using common filters (i.e., Gaussian, median and average) at four kernel sizes (3×3, 5×5, 7×7 and 9×9 pixels) on 4 km SST images prior to the frontal detection. All tests are performed for three different window sizes (16×16, 24×24, 32×32 pixels, hereafter named W16, W24 and W32). Windows sizes smaller than 12×12 pixels were not been tested because of the difficulty of the SIED algorithm finding a statistically valid solution for the separation of two water masses that allows a front to be defined. The tests are also performed without any convolution. A total of 39 window, filter and kernel combinations are evaluated.

The Gaussian filter is used to blur images and partly remove noise. When working with images, it is necessary to use the two-dimensional Gaussian function that is the product of two one-dimensional Gaussian functions (in both x and y directions). The median filter, widely used due to its ability to remove noise while preserving edges, works by computing the median of the neighborhood values. Finally, the average or mean filter reduces the variation between neighboring pixels. The constraints of using this filter includes an excessive influence of outliers pixels on the average, and a blurring effect of the filter in cases of high contrast.

Different smoothing combinations are applied to the 15 test images and fronts are then detected using the CMW method. In order to maximize detections, we adapt the CMW method to 4 km data by altering the internal parameters to $\theta = 0.65$, $S = 3.0$ and $P_{wi} = 0.10$. In particular, a low value of P_{wi} improves the detection of frontal structures closer to the coast. It is important to note that after several tests on 4 km global area coverage data (not shown), we did not apply the "following algorithm" of Cayula & Cornillon (1992) included in the original CMW method, as it did not show a visible improvement of frontal detections at 4 km. Contrary to the original SIED algorithm, no minimum front length has been defined because the CMW method already combines partially detected fronts.

The performance of the frontal detection is evaluated independently for the weak and strong fronts and for each combination of filter, kernel and window size. The performance assessment procedure included a statistical analysis and an expert-based approach. The statistical analysis consisted of the evaluation of: 1) the detection efficiency, defined as the total number of frontal pixels found in each image, and 2) the average length of the fronts (in km), a more complex parameter to define due to potential false breaks between fronts. A "reference" combination (i.e., the smoothing method most frequently used in histogram-based frontal detection studies) is defined as a 3×3 median filter combined with a W32 and is used to evaluate the improvement in the detection efficiency.

Here, we examine front length by first, removing very short fronts (< 10 pixels; considered suspect) from the 15 test images, and then averaging the length of all fronts that have been detected. Next, an expert-based visual examination of the images is performed to account for indicators that are difficult to quantify, such as the shape of the fronts, the proportion of short fronts, the presence of possible "double fronts" and the proximity of fronts to the coastline.

Additionally the histograms of Sobel gradient values associated with fronts are computed for the Moroccan area. This is done to show the effects of the data resolution and the window size on the gradient distribution and to visualize the thresholds used to define the weak and strong fronts. We compare 1) different resolutions (1, 2 and 4 km) using the same window size (W16) and 2) the size of the detection window (16×16, 24×24 and 32×32) at 4 km resolution.

2.4 Performance of the frontal detections

In order to estimate the overall performance of the detections at 4 km, the spatial correspondence between the fronts detected and the gradient is quantified separately for weak and strong fronts. The “representative surface” of each front is first computed by considering a distance of three pixels from all frontal pixels. This is done to account for the precision of the front positioning found to vary from one to three pixels from the nearest maximum corresponding gradient. A detection rate is then calculated from the five clear images of both Moroccan and north-western Australian areas, given as the percentage of fronts that are detected and correspond to either a strong or weak frontal gradient.

2.5 Application of optimal smoothing at the basin scale

To test the optimal smoothing combination found in this study, we apply it at the basin scale in the Indian Ocean on 10 years (2003-2012) of daily 4 km MODIS data. Thermal fronts are detected and monthly frequency of occurrences (in percentage) are mapped and divided into “weak” and “strong” front categories for 1) the north-east (NE) monsoon (December to March) and 2) the south-west (SW) monsoon (June to September). Both monsoon seasons are associated with specific regimes of winds and currents. Biogeographical regions as defined by Longhurst (2007) are superimposed to facilitate visual comparisons of the patterns of frontal occurrence.

The Indian Ocean is known to have specific oceanographic characteristics that differ considerably from the Atlantic and Pacific Oceans, mainly because is bounded in the north by the Asian continent. The thermal contrast between land and sea, due to the presence of the continent, creates a seasonal wind reversal and deep seasonal variability in the ocean currents (Fieux & Reverdin, 2001), making this an ideal ocean to investigate frontal detections.

3. Results and discussion

3.1 Effects of the preliminary smoothing

The results of the preliminary smoothing of the data summarized the combined effects of the filters at different kernel sizes and the effects associated with the size of the detection window. The effects of the internal parameters of the SIED algorithm optimized for 4 km data are minor compared to those of the smoothing type (not shown).

Due to the sensitivity of these factors to the front intensity, or thermal surface gradient, the results are presented here for both "weak" and "strong" front categories.

3.1.1 Frontal detection efficiency

The detection efficiency shows that the impact of the smoothing is considerable. The frontal detections performed without any preliminary convolution (Fig. 2) was much lower than those with a convolution, with very similar results among window sizes (Fig. 2a, b). The higher improvement found in the detection efficiency of the weakest fronts thanks to the smoothing is due to the fact that they are more affected by the spatial noise of the data when using the SIED algorithm than strong fronts. We find that window size shows the biggest effect on frontal detection efficiency, followed by kernel size and filter type.

The effect of the window size is found to be the most important factor for detection efficiency. The average increase compared to the "reference" smoothing (i.e., W32, 3×3 median filter) and the highest detection efficiencies obtained in this study is 71% for strong fronts (using W16, 5×5 median filter) and 120% for weak fronts (using a W16, 7×7 median filter) (Fig. 2a, b). The detection efficiency for weak fronts increased moderately between W32 and W24 (24%) and more strongly between W24 and W16 (68%) (Fig. 2a). The detection efficiency for the strong fronts, increased by 9% from W32 to W24 and by 10% from W24 to W16. Overall, the smallest detection window (W16) gives the highest performance in terms of detection efficiency for both weak and strong front intensities, regardless of the smoothing combinations. The detections made at W16 clearly show the advantage of this unusually small window size, without detection of spurious short fronts as might have been expected. The ability to detect spatially complex fronts, as well as coastal fronts, at this window size, is clearly enhanced relative to W32.

The second dominant factor, after the window size, is the spatial scale of the convolution, i.e., the kernel size. Its effect on detection efficiency is substantial for all window sizes (Fig. 2a, b) and especially pronounced for the smallest window (W16). In general, the effect of the kernel size, is visible for the weakest fronts up to the 7×7 pixel kernel (Fig. 2a) whereas a maximum detection is reached at the 5×5 pixel kernel for the strongest fronts (Fig. 2b).

The three types of filters tested showed different effects on detection efficiency. The Gaussian filter showed a relatively poor performance at W16 except with very large kernel sizes (i.e., 7×7 and 9×9 pixels). These kernels lead to inappropriate detections, such as the presence of double fronts (Fig. 2e, f, right panels), because of their insufficient smoothing efficiency compared to other filters.

At W16, the median filter showed maximum detection efficiencies for kernels 3×3 and 5×5 for strong fronts and 7×7 for weak fronts, decreasing in efficiency thereafter (Table 2). The average filter showed very similar results for W16. Contrary to other filters, the average filter's efficiency increased for higher kernels and window sizes (Fig. 2a). Despite the similar performances of median and average filters, in general, the median filter outperforms the average filter and is hereafter selected as the optimal filter. Visual assessments are consistent with quantitative results (e.g., Fig. 2c-f). The visual improvement using the 5×5 kernel size is obvious for all fronts whereas the 7×7 kernel size slightly enhances the results for the weakest fronts.

Kernel sizes equal to or greater than 7×7 significantly degrade the results for the strong fronts (not shown) with a visible change of their shape. The best detection quality is consequently observed for a smoothing combination using median filter with the 5×5 pixels for strong fronts and 7×7 pixels for weak fronts. We find realistic spatial complexity and remarkably good frontal continuity without spurious double fronts with this combination at W16. This demonstrates the high stability of the CMW detection algorithm

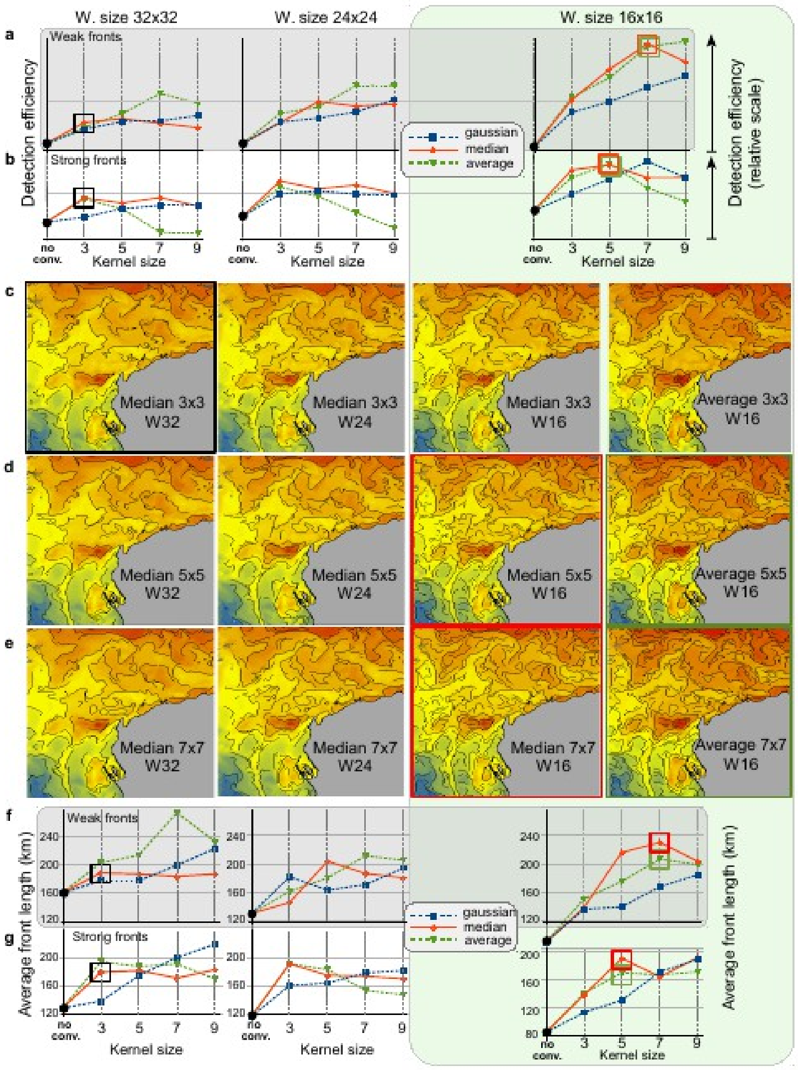

Figure 2. Effects of the preliminary smoothing of 4 km resolution SST data on the front detection. Weak fronts are defined for the gradient interval 0.02-0.042 °C km^{-1} (gray background) and strong fronts for gradients > 0.042 °C km^{-1}. The data correspond to the average of five clear images for each of the three study areas, Morocco, Mozambique Channel and north-western Australia (i.e., totaling 15 images). (a-b) The total number of frontal pixels for the three detection window sizes, 32×32 (left column), 24×24 (middle column) and 16×16 pixels (right column) and the three filters, Gaussian (blue dashed line), median (red line) and average (green dashed line) applied at four kernel sizes, 3×3, 5×5, 7×7 and 9×9 pixels. Data for images where no smoothing was performed are labeled “no conv.” (black dots). The “reference” or standard smoothing (3×3 median W32), generally used in front detection, is represented by black squares. The red and green squares show the best quantitative and visual results for both weak and strong fronts, obtained with median 7×7 and 5×5 respectively. The images show front detections for north-western Australia on November 24th, 2009 for (c) 3×3, (d) 5×5, (e) 7×7 and (f) 9×9 pixel kernel sizes for the the median filter at window sizes of W32 (left column), W24 (middle left column) and W16 (middle right column) and the average filter at the W16 window size (right column).

despite the decrease by a factor of four in the number of pixels analyzed at the window level, compared to the “reference” smoothing for an equivalent 1 km resolution image (see Fig. 4).

3.1.2 Frontal Length

Considerable differences in average front lengths for the 15 test images were found for all window and kernel sizes combinations (Fig. 3a, b). When no convolution was used, front lengths were minimal and the effect of the window size was negligible for both weak and strong fronts. In general, the average lengths were mostly influenced by the large amount of relatively short fronts, which were more numerous with the use of small window sizes.

For weak fronts, front lengths for W24 were similar to W32, but in the absence of smoothing shorter fronts were observed with W24. Distinct local maxima appeared at the 5×5 kernel size for weak fronts and the 3×3 kernel for strong fronts. The influence of the kernel size was even more important for W16, with the highest values for the median and average filters found with the 5x5 kernel for weak fronts and 7×7 kernel for strong fronts (Fig. 3a, b). Front length substantially increased (23%) from W32 to W16, with maximum lengths generally detected for the different convolution using the 7×7 kernel at W16. This is similar to the window and kernel size combinations that find that maximum detection efficiency. On average, fronts associated with strong gradients were 9% longer than those associated with weak gradients. For strong fronts, the average front lengths were very similar across window and kernel sizes .

We find that the smallest detection window (W16) substantially increases the length of the weakest fronts (at both 5×5 and 7×7 kernels) (Fig. 3a). This is observed despite the fact that the geographical size of W16 (72×72 km for a 4.5 km pixel size) theoretically does not allow us to detect fronts longer than 100-150 km. The fact that the average length of the detected fronts is far higher (220 km) and relatively stable between the different window sizes, gives a high degree of confidence in the smoothing method presented, beyond that of the spatial scale of detection. This result is a possible consequence of the CMW procedure that combines four simultaneous detections grids and converges towards stable values of front length, despite the use of different detection scales.

The visual assessment is very helpful to discriminate results that are quantitatively similar. This is particularly the case between the median and average filter types, whose results are very similar in terms of detection efficiency and average front length. Those fronts detected with the average filter appear spatially more complex (Fig. 2c-f rightmost column). These fronts also show a much higher frequency of double fronts that do not correspond to real patterns in the data. The median convolution is not affected by this tendency and can consequently be visually confirmed as the most adequate filter.

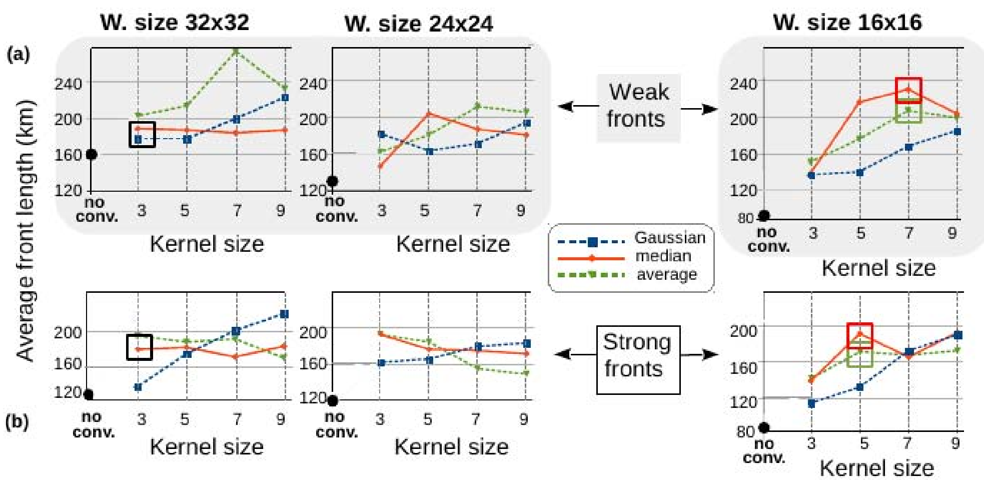

Figure 3. Average frontal length in kilometers for (a) weak and (b) strong fronts, without convolution (black dots) and for each combination of filter type (Gaussian, median and average), kernel (3×3, 5×5, 7×7 and 9×9 pixels) and window size (32×32, 24×24 and 16×16 pixels), as in Figure 2a and b.

Table 2. Summary of sea surface temperature and frontal occurrence spatial and seasonal patterns and their variability for the Aden gulf/ Arabian sea, Bay of Bengal and Eastern South Africa regions (see figure 7 for corresponding two-dimensional fields).

Region / parameter	SPATIAL VARIABILITY (Average)		SEASONAL VARIABILITY (St.dev.)	
	SST (°C)	Frontal occurrence (%)	SST (°C)	Frontal occurrence (%)
Aden Gulf / Arabian sea	Strong spatial variability. with a clear limit between two water masses (27 and 28°C)	**High frontal occurrence (north of Somali and Yemen coasts) No link with SST.**	Strong contrast in variability (Low in Aden Gulf, high in Arabian sea)	**Strong variability where SST variability is low.**
Bay of Bengal	Very weak spatial variability (homogeneous SST ~28.5°C)	**High coastal occurrence without link with SST pattern**	High Coastal variability	**Strong seasonal variations where SST varies (coasts)**
Eastern South Africa	Strong variability, well structured between coastal and oceanic waters.	**Very high and localized occurrence where SST varies**	Very weak and homogeneous variability	**Very weak seasonal variability (similar to SST)**

3.1.3 Global performance of 4 km to 1 km frontal detections

We find that W16 offers the best performance for 4 km due to its high detection power, the stability in front length for kernel sizes > 3×3 pixels and the spatial coherence from the visual assessment. This is found for both front intensities (weak and strong), especially when W16 is associated with median or average filter. We therefore suggest that the optimal smoothing method for preprocessing images uses a median filter with a 7×7 kernel for weak fronts and a 5×5 kernel for strong fronts at W16 (Fig. 2a,b). The detections obtained with this optimal smoothing combination are visually similar to the detections found from independent 1 km resolution images processed with the "reference" combination (Fig. 4a,b).

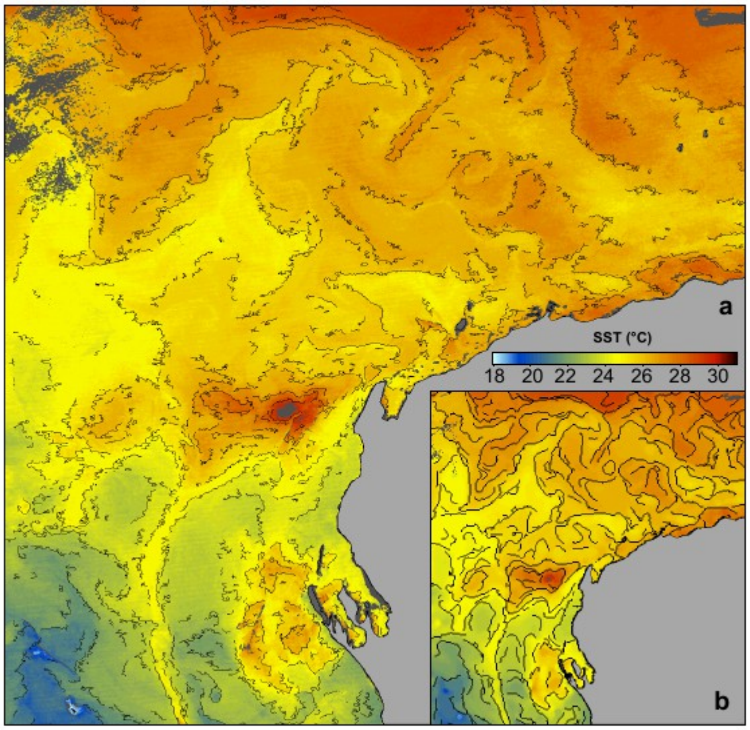

Figure 4. SST and associated fronts detected in November 24th 2009 in north-western Australia at (a) 1 km resolution with standard “reference” parameters (i.e., a median filter with a 3×3 pixel kernel and a window size of 32×32 pixels); and (b) 4 km resolution with the optimal smoothing combination of a median filter with kernel sizes of 5×5 and 7×7 for strong and weak fronts respectively, and window size of 16×16.

Since the shape of the fronts at the near-pixel level change with the spatial scale, its comparison with the frontal detection efficiency of the 4 km data is very difficult. Nevertheless, it is clear that an important quantity of fronts are very well detected on the 4 km data relative to the 1 km data, indicating that the most relevant fronts were detected. Additionally, despite the slightly greater uncertainty in their location induced by the smoothing effect, the spatial distribution of fronts is coherent with 1 km data. Only a minor number of fronts are not detected with 4 km data because of their spatial proximity. This limitation is clearly due to the width of the detection window, despite the fact that we defined a procedure at the lower window size limit permitted by the SIED algorithm. Similar to that observed in the present analysis, Nieblas et al. (2014) found that the CMW algorithm applied to 4 km data missed some fronts relative to 1 km data and that the average frontal length is greater for 4km data than that obtained from 1 km data.

3.1.4 Effects of window size

To illustrate the effect of window size on frontal detections, we computed the average frequency of frontal occurrence to daily (2003-2012) 4 km MODIS SST data offshore of Morocco, applying the optimal preprocessing smoothing of a median filter with 5×5 and 7×7 kernels found above and using the window sizes W16 and W32. Results displayed for February (characterized by moderate coastal upwelling (Barton et al., 1998)) indicate that detections improved from large to small window sizes (based on visual assessments; Fig. 5a, b) mostly in the inner part of the wide continental shelf (Fig. 5c, d), characterized by a previously-defined secondary upwelling front (Makaoui et al., 2005). We also found a homogeneous increase in the frontal occurrence measured by a 120% increase for weak fronts and a 20% increase for strong fronts. In particular, only the smallest window size W16 (Fig. 5b, d) allowed spatially close fronts to be correctly separated, between themselves as well as from the coastline.

Regardless of the window size used (i.e., W16 or W32), coastal patterns of high frontal occurrences were associated with persistent upwelling fronts, mostly originating from the shelf at the vicinity of capes Ghir, Jubi and Bojador and visible with ocean color data (Pacheco & Hernandez-Guerra, 1999). During upwelling events in this region, surface waters are advected away from the coast and generate intense fronts between surface and subsurface layers (Pelegrí et al., 2005). This is especially true south of Cape Ghir where upwelling fronts and filaments are observed far from the coast. Fronts are very concentrated over the continental slope in winter because of the quasi-permanent seasonal thermocline and the slightly lower intensity of the upwelling.

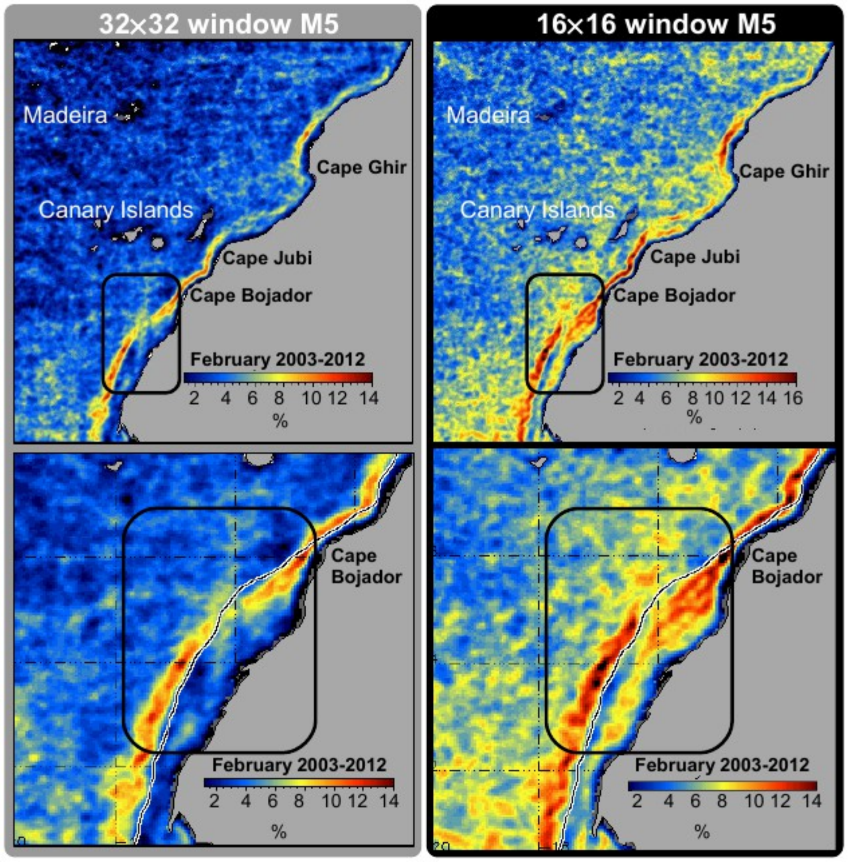

Figure 5. (a-b) Improvement in the detection of thermal fronts between window sizes of 32x32 (left) and 16x16 pixels (right) in the Moroccan upwelling region in February (average 2003-2012) using the optimal smoothing combination of a median filter, kernel sizes of 5×5 for strong fronts and 7×7 for weak fronts. (c-d)The black rectangles highlight the areas where substantial improvements in front detection using the 16x16 window size were observed over the shelf in a complex coastal environment. The 200 m isobath is superimposed in the zoom frames (bottom) .

3.1.5 Effects of the spatial resolution and window size

The Sobel gradient of the SST, which represents one of the most objective evidences of frontal presence, is used to estimate the relative performance of the frontal detections at different spatial resolutions and across window sizes. As previously mentioned, all frontal pixels are by definition associated with a gradient > 0.02°C km^{-1}, in order to reduce the risk of false detection.

For the Moroccan area, approximately 68% of the frontal pixels correspond to gradients above this threshold, which means that 32% of the pixels belong to fronts that do not match the elementary criteria of a front, not even at the weakest possible intensity. This is due to the fact that the SIED algorithm follows a fixed SST threshold value, which does not necessarily correspond to pixels at the same position as the maximum gradient associated with the front.

Therefore, it is interesting to compare the distributions of the SST gradient according to spatial considerations, i.e., data resolution and the size of the detection window. This show that frontal gradients are linearly dependent on the spatial resolution of the data (Fig. 6a), as the minimal spatial resolution of the data (1 km) is far greater than the spatial scale of the *in situ* oceanic fronts. When the gradient distributions are normalized relative to 4 km data, they are very similar in terms of shape (Fig. 6b). In this case, the histogram of the 4 km data only shows slightly more frontal pixels detected relative to 1 and 2 km data for the gradients associated with the strongest fronts and slightly less for the weakest fronts. The gradient distribution at 4 km resolution shows even weaker differences between the different window sizes (Fig. 6c) that are not likely significant.

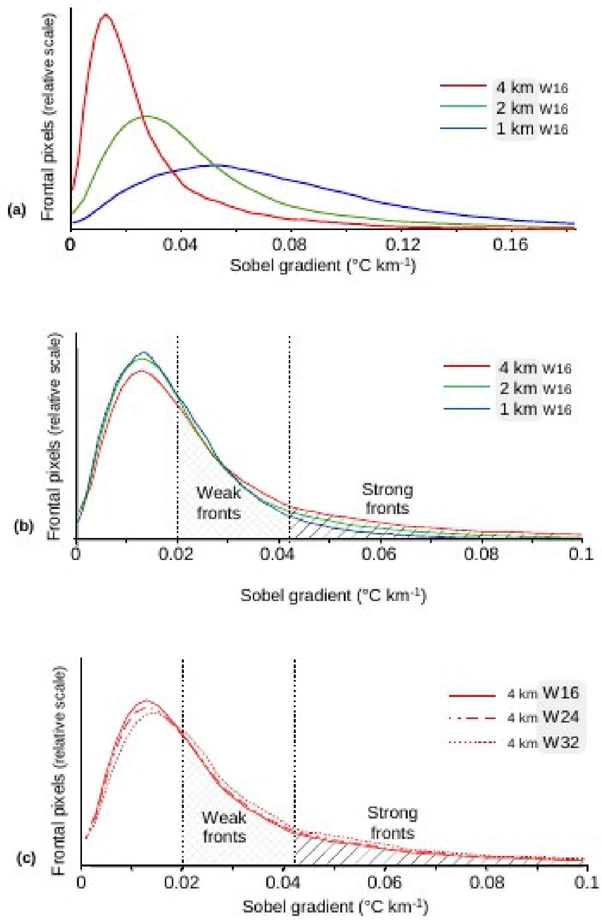

Figure 6. Histograms of the Sobel gradient associated to frontal pixels for the Moroccan region from daily sea surface temperature (SST) data (2003-2012). (a) Sobel gradients for 1 km, 2 km and 4 km SST data for 16x16 pixel window size, (b) SST gradient values normalized relative to the 4 km data gradient scale and (c) SST gradient variability according to the size of the detection window, i.e., 16×16, 24×24 and 32×32. The populations of frontal pixels associated to weak and strong gradients in (b) and (c) are hatched and striped, respectively, while the left of the histograms indicates pixel gradients that are below the 0.02 °C km^{-1} threshold.

3.1.6 Front-gradient validation

Since all images are selected according to their low cloud coverage, all spatially structured gradients are supposed to be real and therefore associated with fronts. Consequently, these gradients (Fig. 7a, b) are used to validate fronts and estimate potentially missing detections and the influence of the window size for both weak and strong fronts.

The detection rates, expressed in percentage, are computed for the Moroccan and the north-western Australian areas (Fig. 7c-n). Detections are similar for both areas when using W16, i.e., 89% (Morocco; Fig. 7e) and 88% (north-western Australia; Fig. 7k) for weak fronts and 93% (Morocco; Fig. 7h) and 91% (north-western Australia; Fig. 7n) for strong fronts These detection rates are 49% and 25% higher for weak and strong fronts, respectively, than those obtained with W32.

The overall proportion of fronts that were not detected dropped from 34% (W32) to 10% (W16): a more than a three-fold decrease. Detection rates between areas and between weak and strong fronts were more similar when using W16 as compared to the larger window sizes, in particular W32. These results indicate that the increase in detection efficiency previously obtained by using W16 (section 3.1.1) corresponds to a validated improvement relative other window sizes. They also confirm the relevance of the optimal preliminary smoothing of the data.

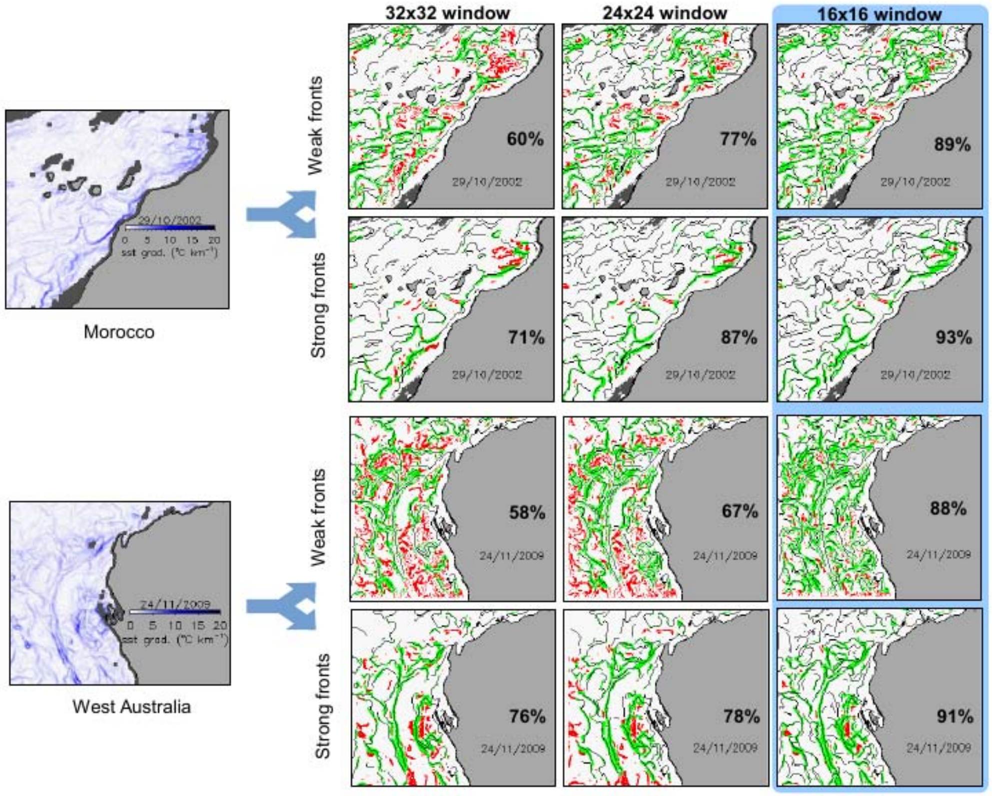

Figure 7. (a,b) Sea surface temperature (SST) gradient values used to validate (c-n) front detections computed from smoothed SST data with a 5×5 median filter for strong fronts and a 7×7 median filter for weak fronts for window sizes 32×32, 24×24 and 16×16 for the Moroccan region (c-h) and north-western Australia (i-n). Percentages are expressed as the proportion of fronts detected associated with both weak and strong gradients (in green) at a maximum distance of three pixels. Frontal pixels that are not associated with an SST gradient are shown in red.

3.2. Large scale application: example of seasonal patterns of frontal occurrence in the Indian Ocean

3.2.1 Weak fronts

During the NE monsoon, a good correspondence is observed between the occurrence of weak fronts and low winds (Fig. 8a and c). Numerous weak intensity fronts with occurrences > 3% are observed from western India to the Arabian Sea during the NE monsoon (Fig. 8c), with the highest occurrences close to the coast. The presence of such fronts in this region may be explained by several factors, such as 1) the effect of the circulation south of Sri Lanka in the exchange of water between the Bay of Bengal and the

Arabian Sea (Reppin et al., 1999), 2) a branch of the westward North Monsoon Current that carries low salinity water from the Bay of Bengal and flows along the west coast of India (Shetye et al., 1991) or 3) the presence of the prevailing north-east trade winds that bring cool, dry continental air to sea, which intensifies the evaporation and leads the surface cooling (Madhupratap et al., 1996).

Front occurrences > 3% are also present around Australia, mainly in the northeastern and southern areas, due to the effect of different currents (e.g., the Indonesian Throughflow, the East Gyral Current, and the Leeuwin Current) in creating boundary fronts in these areas (Fig. 8a, b, c).

During the SW monsoon, weak fronts are far less frequent (< 2%) than during the NE monsoon, especially in the northern Indian Ocean basin (Fig. 8a, b, c right frame). Front occurrences > 3% are only present in the Mozambique Channel, Indonesia and northern Australia. Numerous mesoscale eddies and high eddy kinetic energy in the Mozambique Channel (de Ruijter et al., 2002; Donguy & Piton, 1991; Tew Kai et al., 2009) probably contribute to the high front occurrences observed there. In the eastern basin, the seas around Indonesia and northern Australia are influenced by the South Java Current (SJC), which contributes a north-westward flow during the maximum flow period of the Indonesian Throughflow, which occurs during SW monson (Schott & McCreary, 2001) (Fig. 8 b,c).

3.2.2 Strong fronts

Strong fronts during the NE monsoon with frequencies > 5% (Fig. 8d, left frame) occur in the northern Red Sea, in the coastal area of the Bay of Bengal, in the South China Sea, off southern Madagascar and in the region of the Agulhas Return Current along the Subtropical Convergence Zone. In the northern Bay of Bengal, the activity of the East India Coastal Current and the presence of cyclonic gyres in the southwest part of the bay contribute to front occurrences via coastal upwelling (Vinayachandran & Mathew, 2003).

In southern Madagascar, the front frequency possibly reflects the impact of the South Equatorial Monsoon Current (SEMC) and the presence of a local upwelling (de Ruijter et al., 2002) caused by the westward bend in the East Madagascar Current. Among all fronts investigated in the southern Indian Ocean by Lutjeharms and Valentine (1984), the Agulhas Front is described as having the steepest gradient, associated with a very consistent temperature of 18.4°C. In western Australia, the strong Leeuwin Current, partially supplied by subtropical waters, flows southward and follows the coast around Cape Leeuwin at the southwestern tip of Australia, and beyond 120°E, generating quasi-permanent high intensity fronts. This feature is probably reinforced by the equatorward winds off Western Australia that oppose to the Leewin Current, which is strongest during the NE monsoon (Schott & McCreary, 2001; Schott et al., 2009). Finally, the Subtropical Convergence Zone, between 40°S and 45°S, is characterized by permanent meander fronts, occurring at progressively at higher latitudes east of 80°E.

During the SW monsoon (Fig. 8d, right frame), strong fronts show patterns similar to those found during the NE monsoon, except that fronts of the northern Bengal almost disappear and strong coastal fronts are observed off Somalia, the Aden Gulf and the western Arabian Sea. The Somalian region is impacted by the atmospheric Finlater Jet, which originates from the east African coast (Fieux & Reverdin, 2001) and helps generate the strong Somali upwelling along with the divergence created by the Southern Gyre (Fig. 8b).

In summary, as expected and regardless of season, strong, high intensity fronts frequently occur in coastal regions and in semi-enclosed seas (i.e., the Red Sea and the Persian Gulf). A few regions show weak intensity coastal fronts, i.e., the Arabian Sea and western and southern India during the NE monsoon; and north-western Australia, southern Indonesia and the Mozambique Channel during the SW monsoon. The offshore areas are principally dominated by weak fronts.

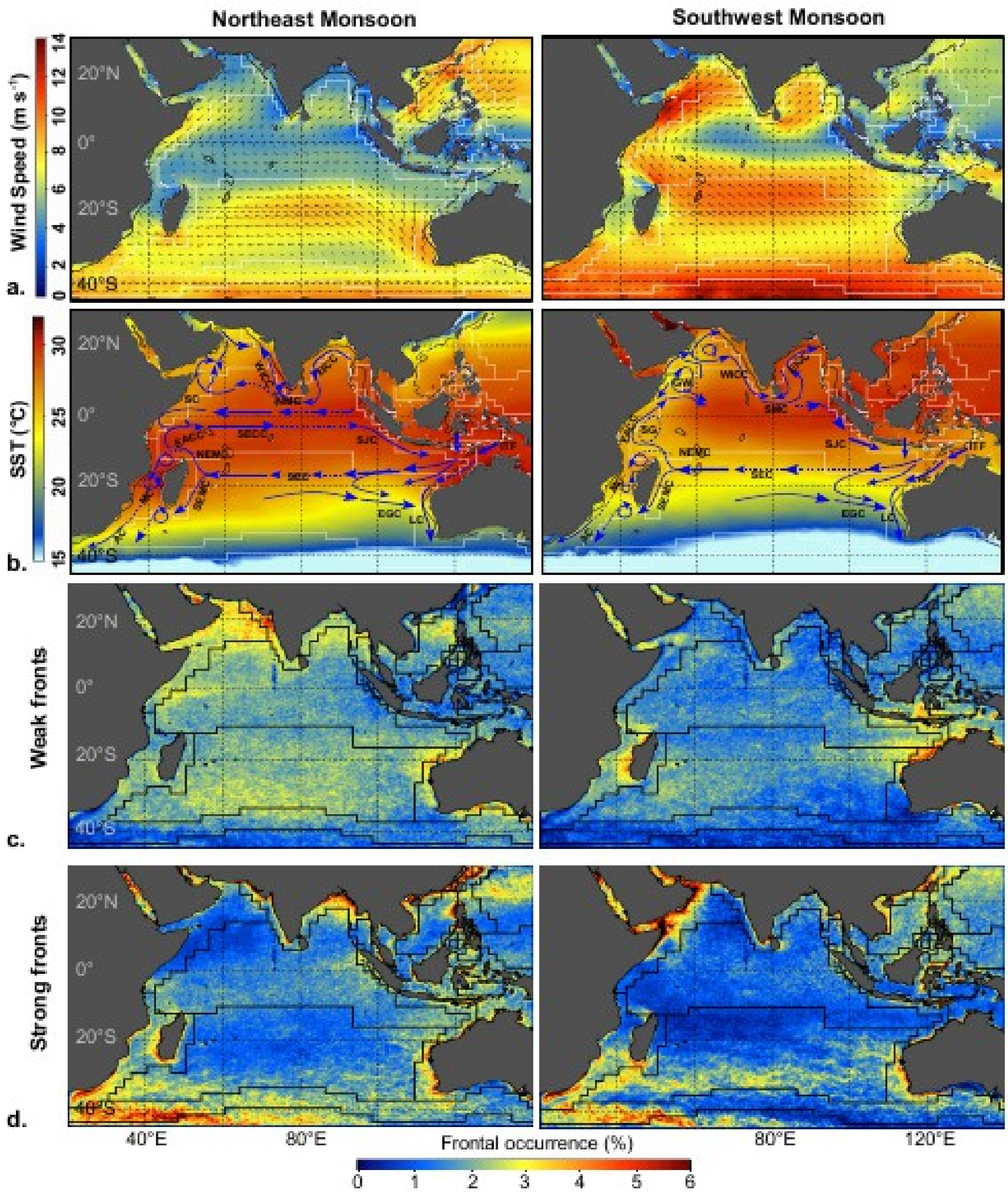

Figure 8. Application of the optimal smoothing combination (median filter, 5×5 kernel for strong fronts, 7×7 kernel for weak fronts, using a detection window of 16x16 pixels) for front detections on 10 years (2003-2012) of daily sea surface temperature (SST) data in the Indian Ocean during the north-east monsoon (December to March) and the south-west monsoon (June to September). (a) Average surface wind field for the same period (Cross-Calibrated Multi-Platform wind product; http://podaac.jpl.nasa.gov/Cross-Calibrated_Multi-Platform_OceanSurfaceWindVectorAnalyses), (b) SST with the main currents (current abbreviations as in Figure 1) and occurrence of thermal fronts of (c) weak and (d) “strong” intensity. The Longhurst (2010) ecological provinces are superimposed.

4. Conclusions

The improvement in the detection of fronts using 4 km data demonstrates the importance of the preliminary spatial smoothing proposed here. The tests performed independently for the two gradient intervals (i.e., weak and strong fronts) confirm that the best results are those obtained by the specific combinations of the following parameters: a median filter, kernel sizes of 5×5 pixels for strong fronts and 7×7 pixels for weak fronts, and a detection window size of 16×16 pixels.

We show that this preliminary smoothing method can be applied to 4 km data at the regional or basin scale levels with comparable results to those obtained using 1 km data. Low resolution data (i.e., 4 km) strongly lightens the constraints related to data manipulation and computing time. We clearly show that major weak and strong fronts are correctly detected and that the frontal continuity is preserved despite the small size of the detection window. A comparable quality of detections is obtained despite the use of sixteen times less data, relative to 1 km resolution images, even if it is clear that 1 km resolution data will always supply more detailed and accurate results.

We observe that strong fronts are mostly found in coastal regions and weak fronts are mostly found in the open ocean. This suggests that the consideration of the frontal intensity may help to spatially differentiate distinct mechanisms of frontogenesis. Over continental shelves, especially in nearshore areas, the methodology proposed here allows us to make a very detailed description of the link between fronts and various physical processes, such as coastal and offshore currents and coastal upwelling.

We selected areas with relatively low cloud cover in order to test the effect of the combinations of parameters of our method on estimating the length and spatial continuity of fronts without constraint or bias due to cloud cover. Otherwise, the Cayula & Cornillon algorithm is not affected by cloud cover, contrary to gradient-based methods. This methodology can be applied in areas with various conditions of cloudiness, including highly clouded regions, such as the Peruvian or Californian coasts, provided that adequate cloud corrections have been previously applied.

Since thermal fronts constitute one of the most important mesoscale features in the ocean, their role in modulating biological productivity (Bainbridge, 1957; Olson & Backus, 1985; Strass, 1992) as well as their direct influence on animal behavior (Laurs et al., 1984; Pakhomov et al., 1994; Polovina et al., 2000; Palacios et al., 2006) is a growing area of interest. The application of this method is potentially useful to better understand, at an ecological level, the association of different organisms with different front intensities as those described here.

Acknowledgments

This study was supported by ICETEX and COLFUTURO funding, from the Colombian government and private enterprises, completed by a third grant from the Agency for Inter-institutional Development Research (AIRD) from the Research Programs and Capacity Building Department of l'Institut de Recherche pour le Développement (IRD), to support students from developing countries. The authors want to thank to Peter Cornillon and Sylvain Bonhommeau for their constructive discussions and advice. We also thank NASA/OBPG for providing the MODIS Aqua data sets used in this study.

5. References

Bainbridge, R. (1957). The Size, Shape and Density of Marine Phytoplankton Concentrations. *Biological Reviews*, *32*(1), 91–115. doi:10.1111/j.1469-185X.1957.tb01577.x

Barton, E. D., Arístegui, J., Tett, P., Cantón, M., García-Braun, J., Hernández-León, S., … Wild, K. (1998). The transition zone of the Canary Current upwelling region. *Progress In Oceanography*, *41*(4), 455–504.doi:10.1016/S0079-6611(98)00023-8

Belkin, I. M., & O’Reilly, J. E. (2009). An algorithm for oceanic front detection in chlorophyll and SST satellite imagery. *Journal of Marine Systems*, *78*(3), 319–326. doi:10.1016/j.jmarsys.2008.11.018

Canny, J. (1986). A Computational Approach to Edge Detection. *IEEE Transactions on Pattern Analysis and Machine Intelligence*, *PAMI-8*(6), 679–698.doi:10.1109/TPAMI.1986.4767851

Cayula, J.-F., & Cornillon, P. (1992). Edge Detection Algorithm for SST Images. *Journal of Atmospheric and Oceanic Technology*, *9*(1), 67–80. doi:10.1175/1520-0426(1992)009<0067:EDAFSI>2.0.CO;2

De Ruijter, W. P. M., Ridderinkhof, H., Lutjeharms, J. R. E., Schouten, M. W., & Veth, C. (2002). Observations of the flow in the Mozambique Channel. *Geophysical Research Letters*, *29*(10), 140–1. doi:10.1029/2001GL013714

Diehl, S. F., Budd, J. W., Ullman, D., & Cayula, J. F. (2002). Geographic window sizes applied to remote sensing sea surface temperature front detection. *Journal of Atmospheric and Oceanic Technology*, *19*(7). doi:10.1175/1520-0426(2002)019%3C1105:GWSATR%3E2.0.CO;2

Donguy, J., & Piton, B. (1991). The mozambique channel revisited. *Oceanologica Acta*, *14*(6), 549–558. Retrieved January 15, 2015, from http://archimer.ifremer.fr/doc/00101/21275/

Fieux & Reverdin. (2001). Current system in the Indian ocean. In J.H. Steele, S. A. Thorpe and K. K. Turekian (Eds). *Encyclopedia of Ocean Sciences* (2nd edition)., Vol. 1, (pp. 728–734). London: Academic Press. doi:f10.1016/B978-012374473-9.00363-5

Gonzalez, R. C., & Woods, R. E. (2007). *Digital Image Processing* (3 edition). Upper Saddle River, N.J: Prentice Hall.

Laurs, R. M., Fiedler, P. C., & Montgomery, D. R. (1984). Albacore tuna catch distributions relative to environmental features observed from satellites. *Deep Sea Research Part A. Oceanographic Research Papers*, *31*(9), 1085–1099. doi:10.1016/0198-0149(84)90014-1

Lutjeharms, J. (2006). The coastal oceans of south-eastern Africa (15,W). In A. R. Robinson & K. H. Brink (Eds.) *THE SEA the global coastal ocean. Interdisciplinary Regional studies and syntheses* (pp 783-831). USA: Library of Congress cataloging-in-Publication data.

Lutjeharms, J. R. E., & Valentine, H. R. (1984). Southern ocean thermal fronts south of Africa. *Deep Sea Research Part A. Oceanographic Research Papers*, *31*(12), 1461–1475. doi:10.1016/0198-0149(84)90082-7

Madhupratap, M., Kumar, S. P., Bhattathiri, P. M. A., Kumar, M. D., Raghukumar, S., Nair, K. K. C., & Ramaiah, N. (1996). Mechanism of the biological response to winter cooling in the northeastern Arabian Sea. *Nature*, *384*(6609), 549–552. doi:10.1038/384549a0

Makaoui, A., Orbi, A., Hilmi, K., Zizah, S., Larissi, J., & Talbi, M. (2005). L'upwelling de la côte atlantique du Maroc entre 1994 et 1998. *Comptes Rendus Geoscience*, *337*(16), 1518–1524. doi:10.1016/j.crte.2005.08.013

Miller, P. (2004). Multi-spectral front maps for automatic detection of ocean colour features from SeaWiFS. *International Journal of Remote Sensing*, *25*(7), 1437–1442. doi:10.1080/01431160310001592409

Miller, P. (2009a). Composite front maps for improved visibility of dynamic sea-surface features on cloudy SeaWiFS and AVHRR data. *Journal of Marine Systems*, *78*(3), 327–336. doi:10.1016/j.jmarsys.2008.11.019

Nieblas, A.-E., Demarcq, H., Drushka, K., Sloyan, B., & Bonhommeau, S. (2014). Front variability and surface ocean features of the presumed southern bluefin tuna spawning grounds in the tropical southeast Indian Ocean. *Deep Sea Research Part II: Topical Studies in Oceanography*. doi:10.1016/j.dsr2.2013.11.007

Nieto, K., Demarcq, H., & McClatchie, S. (2012). Mesoscale frontal structures in the Canary Upwelling System: New front and filament detection algorithms applied to spatial and temporal patterns. *Remote Sensing of Environment*, *123*, 339–346. doi:10.1016/j.rse.2012.03.028

Olson, D. B., & Backus, R. H. (1985). The concentrating of organisms at fronts: A cold-water fish and a warm-core Gulf Stream ring. *Journal of Marine Research*, *43*(1), 113–137. doi:10.1357/002224085788437325

Pacheco, M. M, & Hernandez-Guerra, A. (1999). Seasonal variability of recurrent phytoplankton pigment patterns in the Canary Islands area. *International Journal of Remote Sensing*, *20*(7), 1405–1418. doi:10.1080/014311699212795

Pakhomov, E. A., Perissinotto, R., & McQuaid, C. D. (1994). *Marine Ecology Progress Series. Oldendorf*, *111*(1), 155–169. doi:10.3354/meps111155

Palacios, D. M., Bograd, S. J., Foley, D. G., & Schwing, F. B. (2006). Oceanographic characteristics of biological hot spots in the North Pacific: a remote sensing perspective. *Deep Sea Research Part II: Topical Studies in Oceanography*, *53*(3-4), 250–269. doi:10.1016/j.dsr2.2006.03.004

Pelegrí, J. L., Arístegui, J., Cana, L., González-Dávila, M., Hernández-Guerra, A., Hernández-León, S., … Santana-Casiano, M. (2005). Coupling between the open ocean and the coastal upwelling region off northwest Africa: water recirculation and offshore pumping of organic matter. *Journal of Marine Systems*, *54*(1-4), 3–37. doi:16/j.jmarsys.2004.07.003

Polovina, J. J., Kobayashi, D. R., Parker, D. M., Seki, M. P., & Balazs, G. H. (2000). Turtles on the edge: movement of loggerhead turtles (Caretta caretta) along oceanic fronts, spanning longline fishing grounds in the central North Pacific, 1997–1998. *Fisheries Oceanography*, *9*(1), 71–82. doi:10.1046/j.1365-2419.2000.00123.x

Reppin, J., Schott, F. A., Fischer, J., & Quadfasel, D. (1999). Equatorial currents and transports in the upper central Indian Ocean: Annual cycle and interannual variability. *Journal of Geophysical Research: Oceans*, *104*(C7), 15495–15514. doi:10.1029/1999JC900093

Schott, F. A., & McCreary Jr., J. P. (2001). The monsoon circulation of the Indian Ocean. *Progress in Oceanography*, *51*(1), 1–123. doi:10.1016/S0079-6611(01)00083-0

Schott, F. A., Xie, S.-P., & McCreary, J. P. (2009). Indian Ocean circulation and climate variability. *Reviews of Geophysics*, *47*(1), RG1002. doi:10.1029/2007RG000245

Shetye, S. R., Gouveia, A. D., Shenoi, S. S. C., Michael, G. S., Sundar, D., Almeida, A. M., & Santanam, K. (1991). The coastal current off western India during the northeast monsoon. *Deep Sea Research Part A. Oceanographic Research Papers*, *38*(12), 1517–1529. doi:10.1016/0198-0149(91)90087-V

Strass, V. H. (1992). Chlorophyll patchiness caused by mesoscale upwelling at fronts. *Deep Sea Research Part A. Oceanographic Research Papers*, *39*(1), 75–96. doi:16/0198-0149(92)90021-K

Tew Kai, E., Rossi, V., Sudre, J., Weimerskirch, H., Lopez, C., Hernandez-Garcia, E., … Garçon, V. (2009). Top marine predators track Lagrangian coherent structures. *Proceedings of the National Academy of Sciences*, *106*(20), 8245 –8250. doi:10.1073/pnas.0811034106

Ullman, D. S., & Cornillon, P. C. (2000a). Evaluation of Front Detection Methods for Satellite- Derived SST Data Using In Situ Observations. *Journal of Atmospheric and Oceanic Technology*, *17*(12), 1667–1675. doi:10.1175/15200426(2000)017<1667:EOFDMF>2.0.CO;2

Ullman, D. S., & Cornillon, P. C. (2001b). Continental shelf surface thermal fronts in winter off the northeast US coast. *Continental Shelf Research*, *21*(11–12), 1139–1156. doi:10.1016/S0278-4343(00)00107-2

Vinayachandran, P. N., & Mathew, S. (2003). Phytoplankton bloom in the Bay of Bengal during the northeast monsoon and its intensification by cyclones. *Geophysical Research Letters*, *30*(11), 1572. doi:10.1029/2002GL016717

Wall, C. C., Muller-Karger, F. E., Roffer, M. A., Hu, C., Yao, W., & Luther, M. E. (2008). Satellite remote sensing of surface oceanic fronts in coastal waters off west-central Florida. *Remote Sensing of Environment*, *112*(6), 2963–2976. doi:10.1016/j.rse.2008.02.00707